JACS
JOURNAL OF THE AMERICAN CHEMICAL SOCIETY

Article

pubs.acs.org/JACS

# $Mg^{2+}$ Shifts Ligand-Mediated Folding of a Riboswitch from Induced-Fit to Conformational Selection

Krishna C. Suddala,[†,‡] Jiarui Wang,[‡] Qian Hou,[‡] and Nils G. Walter*[,†,‡]

[†]Biophysics, [‡]Single Molecule Analysis Group, Department of Chemistry, University of Michigan, 930 N. University, Ann Arbor, Michigan 48109, United States

Supporting Information

**ABSTRACT:** Bacterial riboswitches couple small-molecule ligand binding to RNA conformational changes that widely regulate gene expression, rendering them potential targets for antibiotic intervention. Despite structural insights, the ligand-mediated folding mechanisms of riboswitches are still poorly understood. Using single-molecule fluorescence resonance energy transfer (smFRET), we have investigated the folding mechanism of an H-type pseudoknotted preQ$_1$ riboswitch in dependence of $Mg^{2+}$ and three ligands of distinct affinities. We show that, in the absence of $Mg^{2+}$, both weakly and strongly bound ligands promote pseudoknot docking through an induced-fit mechanism. By contrast, addition of as low as 10 $\mu$M $Mg^{2+}$ generally shifts docking toward conformational selection by stabilizing a folded-like conformation prior to ligand binding. Supporting evidence from transition-state analysis further highlights the particular importance of stacking interactions during induced-fit and of specific hydrogen bonds during conformational selection. Our mechanistic dissection provides unprecedented insights into the intricate synergy between ligand- and $Mg^{2+}$-mediated RNA folding.

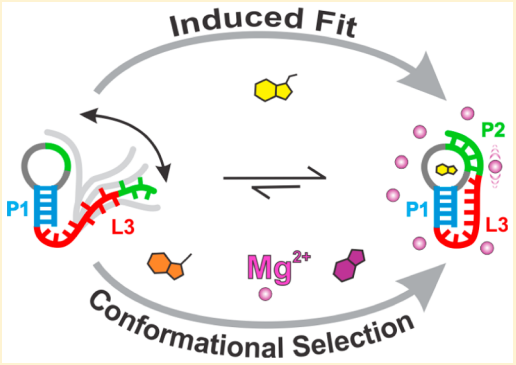


## 1. INTRODUCTION

RNA is remarkable in its ability to recognize a diverse array of small molecules, as exemplified by the recently discovered class of noncoding RNAs known as riboswitches.[1] Riboswitches are highly structured motifs commonly found in the 5′-untranslated regions of bacterial messenger RNAs (mRNAs), where they regulate gene expression mainly through mechanisms such as transcriptional termination and repression of translational initiation.[2] Riboswitches are structurally modular in nature consisting of a ligand binding aptamer domain followed by an expression platform, the conformation of which dictates the level of gene expression. The aptamer domains of riboswitches adopt a variety of architectures and vary greatly in size and complexity.[3] Ligand binding by the aptamer domain stabilizes alternative RNA conformations in the downstream expression platform to turn gene expression either off or on. Gene regulation by riboswitches therefore depends on the efficient folding of the aptamer as mediated by ligand binding. Despite the availability of a diversity of high-resolution structures,[3] our understanding of the molecular mechanisms of the ligand-dependent dynamic folding of riboswitches is far from complete.[4,5]

Molecular recognition processes in general are classified into two distinct mechanisms—induced-fit (IF) and conformational selection (CS)—which are commonly referred to as "binding first" and "folding first" processes, respectively.[5,6] In IF, ligand binding to an unfolded conformation promotes folding, whereas in CS, the ligand selects high-affinity, folded-like structures from an ensemble and thus shifts the conformational equilibrium toward them. Distinguishing these mechanisms with ensemble-averaging techniques has been challenging so that single-molecule probing is rapidly gaining popularity for deciphering coupled binding and folding mechanisms.[5−8] In particular, single-molecule fluorescence resonance energy transfer (smFRET) has been recently used to measure the impact of increasing ligand concentration on the closing and opening rate constants of maltose-binding and ABC transporter proteins as a way to distinguish IF from CS.[9,10]

For riboswitches as a dynamic class of molecules, smFRET microscopy can provide valuable kinetic information about the folding and unfolding structural transitions that are crucial for ligand-dependent modulation of gene expression.[5,11] Consequently, smFRET has been used to investigate the conformational states adopted by various riboswitches and their global dynamics. In most smFRET studies, the effect of the cognate ligand on the structure and dynamics of the riboswitch is investigated in either the presence or absence of $Mg^{2+}$, which serves as the physiologically most relevant cofactor for tertiary structure formation of polyanionic RNA molecules. A common theme emerging from these studies is that $Mg^{2+}$ alone can promote folded-like conformations that are further stabilized significantly upon ligand binding.[4] However, in the absence of a

**Received:** April 10, 2015
**Revised:** September 16, 2015
**Published:** October 15, 2015





DOI: 10.1021/jacs.5b09740
J. Am. Chem. Soc. 2015, 137, 14075−14083

rigorous kinetic analysis of the conformational dynamics at varying ligand concentrations, the folding mechanisms of riboswitches have remained obscure and prone to interpretation based on assumptions.[5] Recently, smFRET investigation of the effector-dependent conformational dynamics in proteins and DNAs showed that folding can be mechanistically dissected using kinetic analysis.[9,10,12]

Here, we have used smFRET kinetic analysis to investigate the coupled ligand binding and folding mechanism of the class-I preQ$_1$ riboswitch aptamer from *B. subtilis* (*Bsu*) (Figure 1a–c).[13,14] The *Bsu* preQ$_1$-I riboswitch is present in the 5′-untranslated region of genes coding for enzymes involved in the biosynthesis of a hypermodified nucleoside, queuosine.[13] Queuosine occupies the anticodon wobble position of certain tRNAs, where it is critical for preventing errors during translation, and is also implicated in bacterial virulence and carcinogenesis in humans.[15,16] The *Bsu* preQ$_1$-I riboswitch senses the intracellular concentrations of the free queuosine intermediates preQ$_1$ (7-aminomethyl-7-deazaguanine) and (possibly) the closely related preQ$_0$ (7-cyano-7-deazaguanine) to terminate transcription of the genes via ligand-mediated stabilization of the aptamer domain.[17] It features the smallest known aptamer domain of just 34 nt length and adopts an H-type pseudoknot fold with helices P1 and P2 and three loops L1–L3 (Figure 1a,b).[17−20] Its small size and elementary structure make this aptamer a preferred model system to understand the molecular underpinnings of riboswitch folding. In a previous smFRET study, we showed that the ligand-free aptamer exists mainly in a prefolded conformational ensemble where the 3′-tail loosely interacts with the P1–L1 hairpin.[21] The aptamer transiently samples a "docked" folded-like structure even in the absence of ligand. On the basis of computational folding predictions suggesting that preQ$_1$ preferentially binds to the docked state, we proposed that this ligand under near-physiological $Mg^{2+}$ conditions primarily binds through the CS (folding first) mechanism.

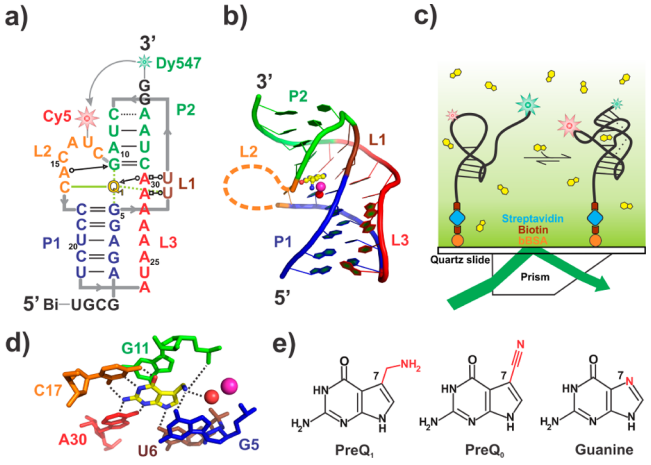


**Figure 1.** smFRET analysis of the preQ$_1$-I aptamer. (a) Secondary structure of the smFRET-labeled *Bsu* aptamer showing key tertiary interactions along with fluorophore labeling positions. (b) Crystal structure of the *Bsu* aptamer (PDB: 3K1V). (c) Schematic diagram of the prism-based smFRET microscopy setup. (d) preQ$_1$ binding pocket showing all hydrogen bonds as broken black lines. The magenta and red spheres represent a bound $Ca^{2+}$ ion and the oxygen atom of its coordinated water molecule, respectively. (e) Structures of ligands preQ$_1$, preQ$_0$, and guanine with differences at position 7 highlighted in red.

In the available crystal and NMR structures, the aptamer binds preQ$_1$ within its core where the ligand stacks between G5 and G11, forms a Watson–Crick base pair with C17, and interacts with U6 of L1 and A30 in L3, using almost all of its available hydrogen-bonding capacities (Figure 1d).[17,18] In addition to its high-affinity ($K_D \approx 20$ nM) cognate ligand preQ$_1$, the *Bsu* aptamer binds the related ligands preQ$_0$ and guanine less tightly with $K_D$ values of ∼100 and ∼500 nM, respectively.[13] The three ligands have distinct hydrogen-bonding capacities around ring position 7, where preQ$_1$ displays a methylamine group, while preQ$_0$ and guanine exhibit a nitrile group and only a ring nitrogen, respectively (Figure 1e). Reasoning that these distinctions may impact the balance between stacking and hydrogen-bonding interactions with the RNA, we compared by smFRET the docking ($k_{dock}$) and undocking ($k_{undock}$) rate constants to probe the coupling of aptamer folding with binding of these three ligands. Most strikingly, we found that ligand-induced folding shifts from the IF to the CS mechanism at $Mg^{2+}$ concentrations as low as 10 $\mu$M.

## 2. RESULTS

**2.1. *Bsu* Aptamer Folds through an Induced-Fit Mechanism in the Absence of $Mg^{2+}$.** The aptamer used for smFRET contained a 5′-biotin, 3′-Dy547, and an internal Cy5 on U19 (Figure 1a,c). This labeling scheme leads to a high-FRET (∼0.9) state in the pseudoknotted structure and a mid-FRET (∼0.65) state in the ligand-free prefolded conformation.[21] Transitions between these two FRET states were observed as before,[21] reporting the rate constants $k_{dock}$ and $k_{undock}$ under a broad range of buffer conditions (Tables S1 and S2). The solution structure of the *Bsu* preQ$_1$-I aptamer was solved in the absence of $Mg^{2+}$, showing that $Mg^{2+}$ is not required for ligand binding by the aptamer.[17] Therefore, we first studied the dynamics of the aptamer in the absence of $Mg^{2+}$ (in a buffer containing 50 mM Tris-HCl, pH 7.5, 100 mM KCl) to probe the binding mechanism and decouple the divalent metal ion's stabilizing effect on the folded conformations from the impact of ligand alone. Individual smFRET traces showed multiple transitions between the two FRET states at varying concentrations of each of the three ligands (Figure 2 and Figure S1). From these smFRET traces, dwell times in each state were extracted and fit well with single-exponential functions to extract $k_{dock}$ and $k_{undock}$ (see Materials and Methods and Figure S3). For preQ$_1$, the $k_{dock}$ value increased from 0.47 $s^{-1}$ at 50 nM to reach a maximum of ∼3.1 $s^{-1}$ at 10 $\mu$M with a hyperbolic dependence on the ligand concentration. A similar trend was observed for the weaker ligands preQ$_0$ and guanine; for preQ$_0$, the $k_{dock}$ value increased from 0.43 $s^{-1}$ at 250 nM to 2.6 $s^{-1}$ at 10 $\mu$M, whereas for guanine, $k_{dock}$ increased from 0.36 $s^{-1}$ at 250 nM to 1.41 $s^{-1}$ at 10 $\mu$M. For all three ligands, $k_{undock}$ remained almost constant with only a marginal decrease at the highest concentrations for preQ$_0$; the average $k_{undock}$ for preQ$_1$, preQ$_0$, and guanine was measured at 0.5, 1.1, and 2.4 $s^{-1}$, respectively. An accelerating $k_{dock}$ and invariant $k_{undock}$ with increasing ligand concentration suggest that, in the absence of $Mg^{2+}$, the *Bsu* aptamer binds all three ligands via the IF mechanism.[5,9,11]

**2.2. $Mg^{2+}$ Promoted Aptamer Folding through a Conformational Selection Mechanism.** Next, we probed the impact of a near-physiological (1 mM) concentration of


DOI: 10.1021/jacs.5b09740
J. Am. Chem. Soc. 2015, 137, 14075−14083

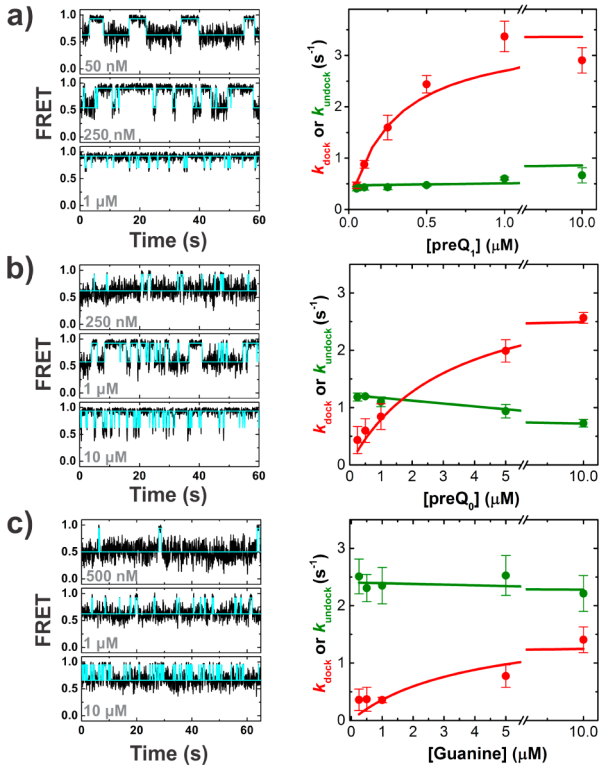


**Figure 2.** Conformational dynamics of the *Bsu* aptamer in the absence of $Mg^{2+}$. (a) Exemplary smFRET traces at increasing preQ$_1$ concentrations (top to bottom). Plot of the preQ$_1$ dependence of the rate constants $k_{dock}$ (red), fit with a noncooperative ($n$ = 1) Hill equation, and $k_{undock}$ (green), fit with a linear regression line. (b) Same as in panel a for preQ$_0$. (c) Same as in panel a for guanine.

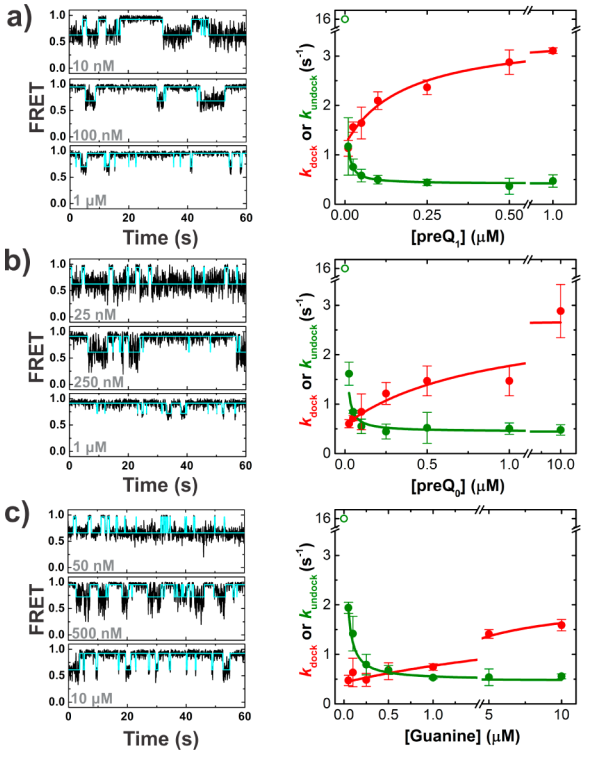


**Figure 3.** Conformational dynamics of the *Bsu* aptamer in the presence of 1 mM $Mg^{2+}$. (a) Exemplary smFRET traces at increasing preQ$_1$ concentrations (top to bottom). Plot of the preQ$_1$ dependence of the rate constants $k_{dock}$ (red), fit with a noncooperative ($n$ = 1) Hill equation, and $k_{undock}$ (green), fit with eq 2 in Supporting Information. (b) Same as in panel a for preQ$_0$. (c) Same as in panel a for guanine. The open green circle represents a lower limit on the $k_{undock}$ value in the absence of ligand derived from cross-correlation analysis.

$Mg^{2+}$, an essential cofactor of tertiary contact formation during RNA folding,[22] on the ligand-dependent folding of the preQ$_1$-I aptamer. $Mg^{2+}$ promotes compact, folded-like aptamer conformations in the absence of ligand (Figure S5).[21,23] In the presence of 1 mM $Mg^{2+}$, the cognate ligand preQ$_1$ increased $k_{dock}$ from ~1.1 $s^{-1}$ at 10 nM to 3.1 $s^{-1}$ at 1 $\mu$M (Figure 3 and Figure S2). Similarly, $k_{dock}$ increased from 0.60 $s^{-1}$ at 25 nM to 2.9 $s^{-1}$ at 10 $\mu$M preQ$_0$ and from 0.47 $s^{-1}$ at 50 nM to 1.6 $s^{-1}$ at 10 $\mu$M guanine. Remarkably, in stark contrast to the no-$Mg^{2+}$ data, the $k_{undock}$ values decreased with increasing concentration for each of the three ligands. Specifically, for the cognate ligand preQ$_1$, $k_{undock}$ decreased from ~1.2 $s^{-1}$ at 10 nM to 0.41 $s^{-1}$ at saturating 1 $\mu$M preQ$_1$. For preQ$_0$ and guanine, the $k_{undock}$ values decreased even more significantly from ~1.6 to 0.42 $s^{-1}$ and from ~2.0 to 0.47 $s^{-1}$, respectively (Figure 3). (We note that heterogenic kinetics were observed both for $k_{dock}$ and $k_{undock}$ in the presence of $Mg^{2+}$, and to some extent for $k_{dock}$ in the absence of $Mg^{2+}$, where data were slightly better fit with double than single exponentials (Figures S3 and S4). Importantly, the average rate constants $k_{dock}$ and $k_{undock}$ from double-exponential fits, while slightly smaller, showed the same differences in folding mechanism as the values obtained from single-exponential fits, which were used throughout for consistency among data sets). This kinetic signature of a ligand-dependent decrease in $k_{undock}$ is a characteristic of CS[5,11,24] and shows that $Mg^{2+}$ shifts the aptamer-folding mechanism for all three ligands toward CS. However, the increase in $k_{dock}$ suggests that IF may also be taking place at higher ligand concentrations, as shown recently,[6,8,25] providing initial evidence that, in the presence of $Mg^{2+}$, both the CS and IF folding mechanisms are operating among the population of molecules.

**2.3. Single-Molecule Transition State Analysis of the Ligand-Mediated Riboswitch Folding.** To gain deeper insights into the differences in the aptamer-folding pathways for the three ligands, we performed single-molecule transition-state analysis (smTSA) of the aptamer folding.[26] TSA (or Φ-value analysis) is a powerful method that has been extensively used to study the nature of protein-folding transition states.[27] By measuring the effect of conservative point mutations on the kinetics and thermodynamics of folding, structural information about the transition state can be probed. For a folding (docking, in this case) reaction, a Φ-value refers to the ratio of the change in the transition-state free energy ($\Delta\Delta G^{\ddagger}_{dock}$) and the change in the equilibrium free energy ($\Delta\Delta G^{0}_{dock}$) of folding between the wild-type and the mutant ($\Phi = \Delta\Delta G^{\ddagger}_{dock}/\Delta\Delta G^{0}_{dock}$).[26] From smFRET experiments, the activation and the equilibrium free energies can be obtained from the individual docking and undocking rate constants as $\Delta\Delta G^{\ddagger}_{dock} = RT \ln (k^{wt}_{dock}/k^{mutant}_{dock})$ and $\Delta\Delta G^{0}_{dock} = RT \ln (K^{wt}_{dock}/K^{mutant}_{dock})$, where $K^{wt}_{dock}$ and $K^{mutant}_{dock}$ are the equilibrium constants for docking in the wild-type and mutant, respectively. A mutation that only accelerates the undocking (unfolding) kinetics without affecting the docking kinetics results in $\Phi = 0$, implying that the contacts made by a residue are not yet formed in the transition state.[26] In contrast, a mutation that decreases docking without affecting undocking leads to $\Phi = 1$, signifying that the tertiary interactions of the residue are fully established


DOI: 10.1021/jacs.5b09740
J. Am. Chem. Soc. 2015, 137, 14075−14083

in the transition state. Therefore, Φ-value provides a measure of the relative formation of the native tertiary interactions in the transition state at the site of mutation. By making multiple mutations at different sites in a molecule, TSA can also be used to model the structure of the folding transition state.[28] For RNA folding, TSA has also been applied, although sparsely, to probe the effect of mutations, metal ions, and denaturants, using both ensemble and single-molecule FRET on a few noncoding RNA structures, but has not yet been applied to riboswitch folding.[26,29]

Although TSA has been extensively used to study the folding of single domain proteins, it can also be applied to investigate bimolecular reactions where folding is coupled to ligand binding.[30] For example, TSA recently has been applied to probe the coupled binding and folding mechanisms of intrinsically disordered proteins (IDPs), protein oligomerization, and aggregation.[31−33] In these studies, mutations were introduced into one of the binding partners and their effects on the nature of the folding transition state were probed. This approach gives information on the structure of the initial "encounter complex", thereby providing insights into the mechanism of folding.[30] We here use a similar approach, albeit the external ligand in our case is a small molecule to which we introduce subtle conservative "mutations".

In our smTSA, we calculated $\Delta\Delta G^0_{dock}$ values that characterize the thermodynamic difference of docking associated with binding the alternate, weaker ligands relative to the cognate ("wild-type") preQ$_1$, as well as $\Delta\Delta G^{\ddagger}_{dock}$ values that reflect the transition-state destabilization by the ligand mutations, all at their respective saturating concentrations. The Φ-values then quantify the fraction of ligand−RNA interactions lost through mutation that were already present in the transition state of preQ$_1$-mediated docking. By measuring the free energies at saturating ligand concentration, this analysis effectively treats the ligand as the integral part of the docked RNA structure that it is. In addition, the use of rate constants at saturating concentrations of all three ligands compensates for the differences in their binding affinities to the aptamer.[13] Because the ligand-binding pocket is fully formed only upon docking of the 3′-tail to the P1−L1 stem-loop to adopt the compact pseudoknot, this analysis effectively quantifies the contacts made by the ligand in the transition state of aptamer folding.

In the absence of $Mg^{2+}$, the values of $k^{\infty}_{dock}$ and $k^{\infty}_{undock}$, which are the rate constants for docking and undocking for the aptamer in the presence of saturating concentrations of preQ$_1$, are 3.46 and 0.50 $s^{-1}$, respectively. This gives an equilibrium constant for docking, $K_{dock} = k_{dock}/k_{undock}$, of ∼6.92 and a free energy of docking, $\Delta G^0_{dock} = -RT \ln (K_{dock})$, of approximately −1.14 kcal/mol (Figure 4a and Table 1). On "mutating" the ligand to preQ$_0$, $k^{\infty}_{dock}$ slightly decreases to ∼3.28 $s^{-1}$ while the $k^{\infty}_{undock}$ value increases almost 2-fold to ∼1.06 $s^{-1}$, resulting in a lower $K_{dock}$ value of ∼3.09. The observation of a similar $k^{\infty}_{dock}$ value for preQ$_0$ as compared to preQ$_1$ and a faster $k^{\infty}_{undock}$ then leads to $\Phi \approx 0.07 \pm 0.02$ (Figure 4a; for a discussion of the accuracy of the smTSA analysis presented here, please see Supporting Information), suggesting that the docking transition states associated with binding the two ligands are nearly identical. This observation implies that the specific ligand−RNA contacts made by the exocyclic 7-methylamine group of preQ$_1$ are not yet formed in the transition state. From the crystal structure, these contacts can be proposed as the one hydrogen bond that 7-methylamine forms with G5 and the pro-Rp oxygen of G11 in P2 (Figure 1d). This finding also supports

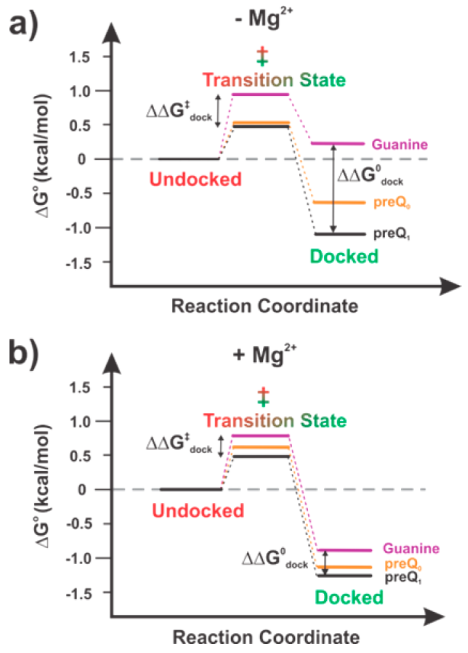


**Figure 4.** Single-molecule transition-state analysis of ligand-dependent riboswitch folding. Free energy diagrams for the ligand-dependent folding of the *Bsu* aptamer in (a) the absence of $Mg^{2+}$ and (b) the presence of $Mg^{2+}$, drawn to scale. $\Delta\Delta G^{\ddagger}_{dock}$ and $\Delta\Delta G^0_{dock}$ for guanine-mediated docking as compared to preQ$_1$ are shown.

the notion that the aptamer folds via IF only after either of the two ligands has already bound to the undocked conformation (primarily via stacking interactions). Similarly, upon binding of guanine, the transition state is only modestly destabilized with ∼2-fold smaller $k^{\infty}_{dock}$ of ∼1.72 $s^{-1}$ as compared to the significant destabilization of the docked state, with a ∼5-fold faster $k^{\infty}_{undock}$ value of ∼2.38 $s^{-1}$, resulting in $\Phi \approx 0.31 \pm 0.15$ (Figure 4a and Table 1). The fact that this value is nonzero may be due to the guanine-mediated transition state lacking a distinct stabilizing feature of both preQ$_1$ and preQ$_0$, such as the van der Waals (stacking) interaction provided by a substituent on ring position 7; alternatively, binding of guanine in the absence of $Mg^{2+}$ may start shifting the folding mechanism toward CS.

Next, we utilized smTSA to probe the folding transition state in the presence of 1 mM $Mg^{2+}$. $Mg^{2+}$ significantly increases the equilibrium constant for docking, $K_{dock}$, for preQ$_0$ and guanine by more than 2-fold and ∼6-fold, respectively, while it only modestly increases preQ$_1$-dependent docking (Table 1). For preQ$_0$ and guanine, this increase in $K_{dock}$ is brought about largely by a significant decrease in the undocking rate constant, $k_{undock}$. smTSA then indicates that the transition-state energies for all ligands shift similarly to those of their respective docked states (Figure 4b), leading to Φ values of $\sim 0.89 \pm 0.25$ and $\sim 0.78 \pm 0.17$ for preQ$_0$ and guanine, respectively. That is, a majority of ligand−RNA interactions are already established in the transition state, rendering it folded-like (docked) and thus primed to bind ligand via CS. Notably, the fractional (nonunity) Φ values provide further evidence consistent with a partitioning of the conformational ensemble into parallel folding pathways, as expected for a mixed CS/IF mechanism in the presence of $Mg^{2+}$ in which a majority, but not all, RNA molecules have largely formed their liganding contacts in the transition state.[6,27]

**2.4. Strong Influence of $Mg^{2+}$ on the preQ$_1$-Mediated Folding Mechanism.** Our kinetic analysis of ligand-depend-


DOI: 10.1021/jacs.5b09740
J. Am. Chem. Soc. 2015, 137, 14075−14083

**Table 1. Rate Constants and Free Energies for smTSA**

| ligand | $k^{\infty}_{dock}$ ($s^{-1}$) | $k^{\infty}_{undock}$ ($s^{-1}$) | $K_{dock}$ | $\Delta G^{0}_{dock}$ (kcal/mol) | $\Delta\Delta G^{0}_{dock}$ (kcal/mol) | $\Delta\Delta G^{\ddagger}_{dock}$ (kcal/mol) | $\phi$ |
|---|---|---|---|---|---|---|---|
| | | | | $-Mg^{2+}$ | | | |
| $preQ_1$ | 3.46 | 0.50 | 6.92 | −1.14 | NA | NA | NA |
| $preQ_0$ | 3.28 | 1.06 | 3.09 | −0.67 | 0.47 | 0.03 | 0.07 ± 0.02 |
| guanine | 1.72 | 2.38 | 0.72 | 0.19 | 1.33 | 0.41 | 0.31 ± 0.15 |
| | | | | $+Mg^{2+}$ | | | |
| $preQ_1$ | 3.44 | 0.41 | 8.39 | −1.25 | NA | NA | NA |
| $preQ_0$ | 2.83 | 0.42 | 6.73 | −1.12 | 0.13 | 0.12 | 0.89 ± 0.25 |
| guanine | 2.10 | 0.47 | 4.47 | −0.88 | 0.37 | 0.29 | 0.78 ± 0.17 |

ent conformational dynamics showed that, under a near-physiological $Mg^{2+}$ concentration of 1 mM, the folding mechanism shows features of CS as evident from the decreasing $k_{undock}$ at higher ligand concentrations (Figure 3), in contrast to the IF mechanism at zero $Mg^{2+}$. To find the $Mg^{2+}$ concentration where the shift from IF to CS occurs, we determined the rate constants of docking and undocking for the cognate ligand $preQ_1$ at the three intermediate $Mg^{2+}$ concentrations of 1, 10, and 100 $\mu$M (Figure 5). Under all

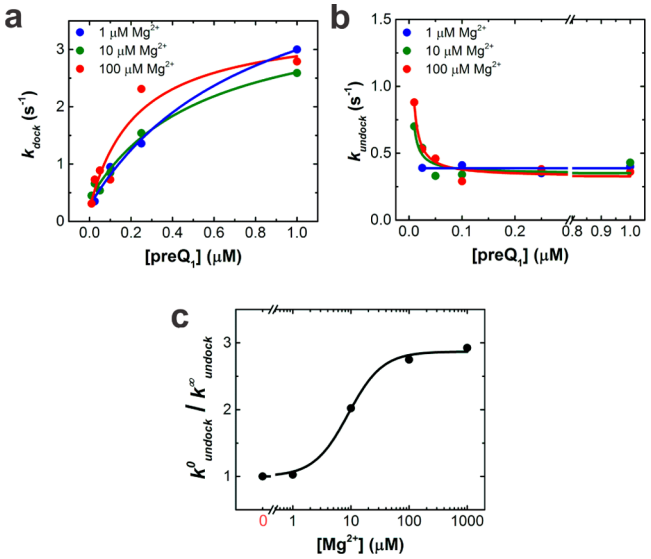


**Figure 5.** Effect of $Mg^{2+}$ on (a) $k_{dock}$ and (b) $k_{undock}$ as a function of $preQ_1$ concentration. The curves represent noncooperative ($n$ = 1) Hill-equation fits to the data at varying $Mg^{2+}$ concentrations as indicated. (c) Semilogarithmic plot of the ratio $k^{0}_{undock}/k^{\infty}_{undock}$ against the $Mg^{2+}$ concentration, fit with a Hill equation with a fixed $y$-intercept of 1, yielding a saturation ratio of ~2.9, a $K_{1/2}$ for $[Mg^{2+}]$ of 9 ± 1 $\mu$M, and a cooperativity coefficient of $n$ = 1.47. The first point in the plot (left of the axis break, colored in red) is showing the zero $[Mg^{2+}]$ value.

three conditions, the $k_{dock}$ value increases hyperbolically with ligand concentration, as also observed in the absence of $Mg^{2+}$ and at 1 mM $Mg^{2+}$ (Figure 5a). By contrast, $k_{undock}$ at 1 $\mu$M $Mg^{2+}$ is independent of the $preQ_1$ concentration (Figure 5b), similar to the $Mg^{2+}$-free condition (Figure 2a), but from 10 $\mu$M $Mg^{2+}$ the characteristic trend starts to appear of a decreasing $k_{undock}$ with increasing ligand concentration. Finally, at 100 $\mu$M $Mg^{2+}$ this trend is as pronounced as in the presence of 1 mM $Mg^{2+}$ (compare Figure 5b and Figure 3a). These observations suggest that $preQ_1$-mediated folding shifts from the IF to the CS pathway across the riboswitch population at $Mg^{2+}$ concentrations significantly below 1 mM. To derive an estimate for the half-titration point $K_{1/2}$, we plotted the ratio $k^{0}_{undock}/k^{\infty}_{undock}$ at the different $Mg^{2+}$ concentrations as shown in Figure 5c. The data, when fit with a Hill equation with $y$-intercept of 1 (since $k_{undock}$ is independent of the $preQ_1$ concentration at zero $Mg^{2+}$), showed saturating behavior even at 100 $\mu$M $Mg^{2+}$ and yielded a $K_{1/2}$ of 9 ± 1 $\mu$M $Mg^{2+}$, with a cooperativity constant of $n$ = 1.47. These findings suggest that at least one high-affinity $Mg^{2+}$ ion is required for 3′-tail docking to form the folded state ensemble that the ligand selectively binds during the CS mechanism.

## 3. DISCUSSION

Folding of riboswitches is intricately linked to ligand binding.[5,11] Such coupled binding and folding mechanisms are crucial for effective gene regulation, especially for riboswitches functioning at the level of transcription termination that entails kinetic competition between alternate folding and transcription.[34] Although the folding of proteins coupled to ligand binding is actively investigated, similar studies on RNA are relatively few. Over the past decade, our understanding of the molecular mechanisms employed by RNA to recognize a chemically diverse array of ligands was advanced by a wealth of high-resolution crystal structures of various riboswitch classes bound to their ligands.[1] In contrast, only a few structures of ligand-free riboswitches were successfully solved, offering limited insights into the plausible ligand-binding mechanisms of riboswitches.[3,35] These structures likely represent only a subset of compact, crystallizable conformations of a large ligand-free ensemble sampled by the RNA, as suggested by lower-resolution solution measurements (such as small-angle X-ray scattering (SAXS)).[35] In addition, static crystal structures cannot explain the mode of transition from a ligand-free (apo) conformation to the ligand-bound (holo) conformation that is crucial to understanding riboswitch mechanism and function.[4] NMR spectroscopy has been used to probe the conformations sampled by riboswitches and to study ligand-binding mechanisms.[23,36,37] Recently, smFRET microscopy has emerged as a powerful tool to characterize the structure, dynamics, and ligand-induced folding of riboswitches.[5,11,38] In the present study, we have performed a smFRET-based kinetic analysis of the $preQ_1$-I aptamer from *B. subtilis* to probe the influence of $Mg^{2+}$ on the folding mechanism in the presence of ligands of varying affinities.

Our results demonstrate that physiological $Mg^{2+}$ concentrations govern the folding pathway of the *Bsu* aptamer toward its native ligand-bound state. On the basis of our smFRET kinetic and transition-state analyses, we propose a model in which ligand and $Mg^{2+}$ synergistically fold the *Bsu* aptamer (Figure 6). In the absence of $Mg^{2+}$ and ligand, the aptamer largely exists in an unfolded hairpin conformation, as previously suggested from smFRET analysis of the *Bsu* aptamer and


DOI: 10.1021/jacs.5b09740
J. Am. Chem. Soc. 2015, 137, 14075−14083

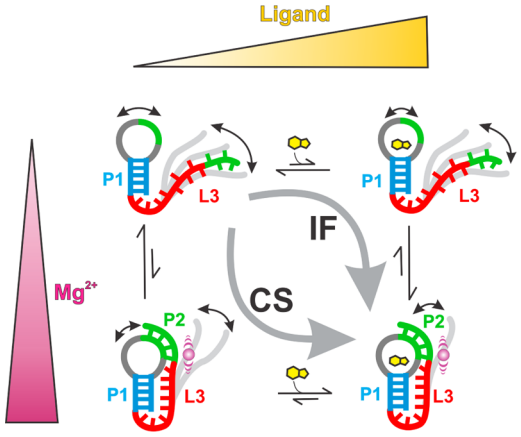


**Figure 6.** Model of synergistic ligand- and $Mg^{2+}$-mediated folding of the *Bsu* aptamer. In the absence of $Mg^{2+}$, the aptamer mainly exists in an unfolded hairpin conformational ensemble (the gray lines and the double-headed arrows are drawn to convey the dynamic nature of the ensemble). Ligand (yellow) binding to this unfolded conformation promotes folding via the IF pathway. In the presence of $Mg^{2+}$, the aptamer samples compact, loosely pseudoknotted, folded-like conformations that are captured via CS and further stabilized by the ligand. High ligand concentrations favor IF, whereas CS dominates at high $Mg^{2+}$ concentrations due to the increased population of compact conformations.

shown by NMR for a similar $preQ_1$-I aptamer from *F. nucleatum* (*Fnu*).[21,23] Under these conditions, the aptamer folds through IF where the ligand binds first to an open (undocked) conformation of the RNA, followed by pseudoknot folding over the ligand. This is further supported by previous NMR observation that $preQ_1$ can remain bound to a conformation in which the upper stem P2 is unstable or not formed.[39] By contrast, upon addition of $Mg^{2+}$, folded-like conformations become more populated (i.e., $Mg^{2+}$-stabilized) if still transient[21,23] and are captured and further stabilized by the ligand through CS (Figure 6). Such a CS-like folding mechanism was recently proposed for the *Fnu* $preQ_1$-I aptamer based on indirect evidence from ensemble-averaged NMR relaxation dispersion experiments,[36] but we show here that both IF and CS likely coexist and are only relatively more or less favored depending on the specific experimental conditions, especially the $Mg^{2+}$ concentration. For the *Bsu* $preQ_1$-I aptamer, our data suggest that a significant flux goes through the CS pathway at $Mg^{2+}$ concentrations as low as ~9 $\mu$M (Figure 5), evidenced by a decreasing $k_{undock}$ with increasing ligand concentration. Although the exact mechanism for the observed stabilizing effect of $Mg^{2+}$ on the docked conformation is not known, we note that a site-specifically bound $Ca^{2+}$ ion near the helix P2, where loop L1 kinks sharply (Figure 1b), was found in the crystal structure and also detected by NMR.[39] Furthermore, small chemical shifts were observed near the $Ca^{2+}$ binding site in the presence of $Mg^{2+}$, suggesting that $Mg^{2+}$ ions interact with this region albeit less site-specifically. Moreover, $Pb^{2+}$ footprinting detected a potential $Mg^{2+}$ binding site in a homologous *Fnu* $preQ_1$-I aptamer, in the loop region near the base of P2.[40] We posit that the observed ligand-dependent decrease in $k_{undock}$ in the presence of $Mg^{2+}$ is most likely achieved through largely nonspecific, yet high-affinity, electrostatic interactions[22] of the P2 stem and/or loop L2 with 1−2 divalent metal ions needed for 3′-tail docking prior to ligand binding.

$Mg^{2+}$ in general is known to promote fluctuations in riboswitches in the absence of ligand into compact native-like conformations that it then stabilizes;[4,37] once sufficiently stabilized, these conformations can form the basis for CS by the ligand. Indirect evidence exists that even small differences in aptamer sequence and $Mg^{2+}$ concentration may have a significant effect on the nature of the ligand-mediated folding mechanism. For example, while kinetic data suggest an IF mechanism for the *pbuE* adenine riboswitch in 0.5 mM $Mg^{2+}$, the structurally similar *xpt* guanine riboswitch was proposed to follow a CS model in 1 mM $Mg^{2+}$.[5] Similarly, we suggested that the structurally highly similar *Bsu* and *Tte* $preQ_1$-I riboswitches to fold through distinct CS and IF mechanisms in 1 mM $Mg^{2+}$, respectively.[21] Our finding of an exquisite sensitivity of the folding mechanism of the *Bsu* riboswitch to the $Mg^{2+}$ concentration, with a transition from IF to CS folding around just 9 $\mu$M (Figure 5c), is arguably a particularly poignant example of such fine-tuning.

The observation of a $Mg^{2+}$-promoted CS mechanism for the folding of the *Bsu* aptamer also raises the question of how a ligand reaches its binding pocket for which crystal and NMR structures reveal a largely buried solvent-accessible surface area.[17,18] Studies of enzymes containing a "lid" over their substrate binding sites have shown that the presence of even a small population of partially closed, ligand-free conformations are sufficient for the folding to proceed through either CS or IF mechanisms.[6] In analogy, NMR studies of the *Bsu* aptamer have indicated that loop L2 is highly dynamic in the pseudoknot conformation, which is also supported by its missing density in the crystal structure, and may thus act as such a lid on the binding pocket in a loose pseudoknot with an almost completely formed P2.[18,39]

From the limited mechanistic smFRET studies of riboswitches, no consensus has yet emerged between the mode of gene regulation and the mechanism of ligand binding.[5] Transcriptionally acting riboswitches are thought to be kinetically controlled, where the ligand-mediated conformational change has to occur cotranscriptionally within a narrow time window before RNA polymerase passes the intrinsic terminator hairpin.[34] For such a riboswitch under kinetic control, an IF mechanism may be advantageous since the rate of folding upon ligand binding may be significantly faster than the rate of transient fluctuations of ligand-free conformations during CS. In addition, for transcriptionally acting riboswitches the ability during IF to weakly bind the ligand even before the entire aptamer domain has been completely transcribed may provide extra time to commit to a gene regulatory decision. In the case of the transcriptional *Bsu* $preQ_1$-I riboswitch studied here, the distance between the 3′-ends of the aptamer and the terminator hairpin is ~25 nt, leaving a time window of only ~1 s within which the ligand-bound pseudoknot has to stably fold to terminate transcription. Our observation of similarly fast pseudoknot docking/undocking kinetics under physiological $Mg^{2+}$ concentrations (Figure 3), which may be further accelerated under the crowded molecular conditions found in vivo, suggests that the IF mechanism can in fact be suitable for such fast transcriptional regulation.[39]

While the cognate ligand $preQ_1$ with the highest affinity showed a relatively small decrease in $k_{undock}$ with increasing ligand concentration, the weaker near-cognate ligands $preQ_0$ and in particular guanine showed more significant decreases (Figure 3). This is consistent with the notion that, under conditions where both open and closed conformations of the


DOI: 10.1021/jacs.5b09740
J. Am. Chem. Soc. 2015, 137, 14075−14083

RNA coexist, the weaker the ligand, the more it binds via CS, where compact, partially closed, high-affinity conformations are selected from the ensemble over low-affinity open conformations from which the weak ligand presumably dissociates too rapidly for IF to occur.[41]

Fractional Φ-values as obtained in our smTSA (Figure 4) are classically interpreted to correlate with the degree of native contacts formed in a transition state.[27] More precisely, such a fractional Φ-value represents an average value for the transition-state ensemble (TSE) derived from parallel folding pathways and gives a measure of the closeness of the TSE to the folded state. Evidence for multiple folding pathways also can be found in the mildly heterogeneous kinetics observed in our data, which are more pronounced in the presence of $Mg^{2+}$ (Figures S3 and S4). In fact, tight $Mg^{2+}$ binding sites are thought to be a major cause of heterogeneous folding of nucleic acid structures containing helical junctions and/or loops.[42−44] Our *Bsu* aptamer contains three loops of varying sizes, with an extended loop L2 that is atypical of H-type pseudoknots.[18] Differential occupancy of $Mg^{2+}$ around these loops and P2 could thus cause the observed heterogeneous kinetics.[42−44] In contrast, the small heterogeneity mostly in $k_{dock}$ in the absence of $Mg^{2+}$ may stem from a ligand-free open conformation that exists as a broad ensemble exhibiting different degrees of P1−L1 interaction with the 3′ A-rich tail, as suggested by our previous smFRET studies.[21] Notably, our use of average rate constants from single-exponential fits then yields insights into the nature of the overall folding mechanism that can be related with those obtained from classical, ensemble-averaging kinetic measurements.[30]

Previous smFRET studies on riboswitches only probed the influence of the single cognate ligand on the folding pathway.[5] However, cells contain many closely related metabolites at concentrations similar to or higher than the cognate ligand. In certain cases, it was suggested that noncognate ligands with lower affinity can in principle bind to and affect the gene regulation of riboswitches.[13] Our work directly addresses this notion for the $preQ_1$-I riboswitch. Interestingly, our kinetic data show that in the absence of $Mg^{2+}$ the equilibrium constant for docking, $K_{dock}$, follows the expected trend of binding affinities, with $preQ_1$ > $preQ_0$ > guanine (Figure 4a).[13] While $K_{dock}$ in the presence of near-physiological $Mg^{2+}$ follows a similar trend, the difference between the ligands decreases significantly, with the nearest noncognate ligand $preQ_0$ adopting an equilibrium constant similar to that of $preQ_1$ (Figure 4b). This suggests that, under in vivo conditions, $preQ_0$ may stabilize the native conformation of the riboswitch to act as a "proxy" for $preQ_1$. Given that $preQ_0$ is an immediate upstream intermediate of $preQ_1$ in the biosynthetic pathway controlled by the riboswitch in its entirety, such redundancy may serve the role of more robustly regulating gene expression.

Distinguishing the IF and CS folding mechanisms traditionally has been difficult using ensemble methods so that many studies have incorrectly posited that folding occurred via a CS mechanism based solely on the observation of folded-like conformations in the absence of ligand.[6,45] Importantly, it has been noted that studying the effects of ligand on the relaxation kinetics of (un)folding ($k_{obs}$) using ensemble experiments cannot unambiguously distinguish between the two mechanisms.[8] By contrast, single-molecule techniques, including force spectroscopy using optical tweezers and smFRET as demonstrated here, are ideal tools for dissecting the individual rate constants $k_{dock}$ and $k_{undock}$ and thus for directly unraveling the ligand binding mechanism(s). We have introduced smTSA to further strengthen our conclusions while highlighting the importance of stacking interactions during IF when the ligand binds to the open (undocked) conformation, as well as of specific hydrogen bonds during CS when the ligand binds to the folded-like (docked) conformation of the $preQ_1$ aptamer. Future three-color smFRET studies employing a ligand labeled with a third fluorophore or a dark quencher may be applied to visualize the arrival time of the ligand relative to pseudoknot docking.[9] However, labeling may be nontrivial to accomplish because most ligands are tightly shielded in their RNA binding pockets so that fluorophore appendages may easily interfere with binding. For certain riboswitches, such as the hydroxocobalamin riboswitch, the ligand itself acts as a quencher and, therefore, can report on the nature of the ligand-binding conformation at the single-molecule level.[46] Alternatively, ensemble flux calculations using rigorous analysis of kinetic measurements could be carried out but have only been applied recently to study ligand-binding coupled protein folding.[25,41]

In summary, we have shown that combined kinetic and transition-state analyses using smFRET are a powerful toolset to dissect the exquisite interdependence of ligand- and $Mg^{2+}$-mediated folding mechanisms of a riboswitch. We anticipate that this work will pave the way for deciphering the coupled ligand binding and folding pathways of many riboswitch RNAs, which will render them attractive antibiotic drug targets.

## 4. MATERIALS AND METHODS

**4.1. Labeling and Purification of RNA.** The *Bsu* $preQ_1$-I riboswitch aptamer[13,21] with the sequence 5′-*UGCGGG***AGAGGUUCUAGC(5-N-U)ACACCCUCUAUAAAAAACUAA***GG*-3′ was chemically synthesized by Dharmacon, Inc. (Fayette, Colorado) with a 5′-biotin, 3′-Dy547, and an internal 5-aminoallyl uridine (5-N-U) at U12. The sequence shown in bold is the minimal aptamer construct that was crystallized, and the numbering used is consistent with this construct.[18] The RNA was deprotected following the manufacturer's protocol and labeled with Cy5-NHS ester (GE Healthcare) as previously described.[21] Excess dye was removed using a NAP-5 gel filtration column (GE Healthcare) followed by ethanol precipitation. The doubly labeled RNA was dissolved in autoclaved, deionized water and used for performing smFRET experiments.

**4.2. Single-Molecule FRET.** Single-molecule FRET experiments were performed using prism-based total internal reflection fluorescence (TIRF) microscopy.[11,14] The doubly labeled RNA with a 5′-biotin was immobilized onto the surface of clean quartz slides containing a microfluidic channel using the biotin−streptavidin interaction. Prior to immobilization, the aptamer was folded by heating a low concentration (20−50 pM) of RNA at 90 °C for 1 min in 1× smFRET buffer (50 mM Tris-HCl, pH 7.5, 100 mM KCl) without $Mg^{2+}$ and allowed to slowly cool down to room temperature over 15 min. The heat-annealed RNA was used for immobilization onto the slide surface, and the unbound molecules were washed away using the 1× smFRET buffer ($\mp Mg^{2+}$). Ligand titrations were performed on the same slide in the 1× smFRET buffer with or without 1 mM $Mg^{2+}$. An enzymatic oxygen scavenging system consisting of 5 mM protocatechuic acid (PCA), protocatechuate-3,4-dioxygenase (PCD), and 2 mM Trolox (6-hydroxy-2,5,7,8-tetramethylchroman-2-carboxylic acid) was used to extend the life of fluorophores and to reduce photoblinking.[21,47] Molecules were imaged at ∼16 Hz time resolution using an intensified charge-coupled device camera (ICCD, I-Pentamax, Princeton Instruments). A 532 nm green laser was used to excite Dy547, and fluorescence from both Dy547 and Cy5 were recorded from which FRET efficiency was calculated as $I_A/(I_D + I_A)$, where $I_D$ and $I_A$ stand for the background-corrected intensities of Dy547 (donor) and Cy5 (acceptor), respectively. Raw movies were processed using IDL (Research Systems, Inc.) to generate smFRET time traces that were further analyzed using custom written


DOI: 10.1021/jacs.5b09740
J. Am. Chem. Soc. 2015, 137, 14075−14083

MATLAB (The Math Works) scripts. smFRET traces displaying single-step photobleaching, a signal-to-noise ratio of >4, and a total fluorescence intensity ($I_D + I_A$) of >300 (arbitrary units) were manually selected for kinetic analysis. The traces were idealized with a two-state model using hidden-Markov modeling (HMM) with a segmental $k$-means algorithm as implemented in the program QuB.[48,49] Dwell times in the undocked and docked states were extracted from all the idealized traces, and the cumulative dwell time distributions were fit with a single-exponential function to obtain the rate constants $k_{dock}$ and $k_{undock}$, respectively. A minimum of 70 smFRET traces showing multiple transitions were included for kinetic analysis for every experiment so that more than 250 dynamic traces were used to obtain the mean and standard deviation (SD) of all the rate constants. Heterogeneity in the kinetic behavior was observed in some conditions, mainly in the docking rates in the presence of $Mg^{2+}$. In such cases, fitting with a single-exponential function reports an average rate constant value. Ligand-titration experiments in the presence or absence of $Mg^{2+}$ were performed for each ligand in triplicates, and the mean ± SD for the rate constants were plotted as Figures 2 and 3. Cross-correlation analysis of the smFRET traces in the absence of ligand was performed as described previously.[50]

**4.3. Single-Molecule Transition-State Analysis (smTSA).** Single-molecule transition-state (or Φ-value) analysis was carried out as previously described.[26] The rate constants of docking and undocking at saturating ligand concentrations $k^{\infty}_{dock}$ and $k^{\infty}_{undock}$ were used to calculate the changes in free energy barrier for docking, $\Delta\Delta G^{\ddagger}_{dock}$, and the overall equilibrium stability, $\Delta\Delta G^{0}_{dock}$, of preQ$_0$- and guanine-bound complexes as compared to the preQ$_1$-bound RNA at 295 K. The $k_{dock}$ versus $[L]$ data in the absence or presence of $Mg^{2+}$ as shown in Figures 2 and 3 were fit with the following single-site (noncooperative) binding Hill equation to yield $k^{0}_{dock}$:

$$k_{dock} = \frac{[L] \times (k^{\infty}_{dock} - k^{0}_{dock})}{[L] + K_{1/2}} + k^{0}_{dock} \quad (1)$$

In the absence of $Mg^{2+}$, the ligand-free preQ$_1$-I aptamer exists mainly in a hairpin conformation without any tertiary interactions as shown by NMR and supported by our previous smFRET analysis, indicating that the molecules exist mainly in a static ∼0.6 FRET state with a negligible $k^{0}_{dock}$.[17,21,23] The values of $k^{\infty}_{dock}$, the docking rate constant at saturating $[L]$, were obtained from fitting the data using eq 1.

The $k_{undock}$ vs $[L]$ data in the absence of $Mg^{2+}$ were fit using linear regression, and the average value of $k_{undock}$ was used for the calculation of Φ-value. The data showing decrease in $k_{undock}$ in the presence of $Mg^{2+}$ were fit with the following equation,

$$k_{undock} = \frac{k^{0}_{undock}}{1 + [L]/K_{1/2}} + k^{\infty}_{undock} \quad (2)$$

which describes the decrease in $k_{undock}$ with increasing $[L]$ for the CS mechanism of folding, where $k^{0}_{undock}$ and $k^{\infty}_{undock}$ refer to $k_{undock}$ at $[L]$ = 0 and at $[L] = \infty$ (saturating $[L]$), respectively.[6,24] An additional $k^{\infty}_{undock}$ term was included in the equation to account for the nonzero undocking rate observed even at saturating $[L]$. The value of $k^{0}_{undock}$ was estimated from cross-correlation analysis of smFRET traces in the presence of 1 mM $Mg^{2+}$ alone, where a majority of the smFRET traces were static.[21] However, a small fraction (∼20−30%) showed fast transitions close to the time resolution (∼16 Hz) of the camera (Figure S5), from which an average combined rate constant (from 20 traces) $k_{dock} + k_{undock}$ of ∼12.24 $s^{-1}$ was obtained that likely represents a lower limit for the rate constant of structural transition. Therefore, the value of $k^{0}_{undock}$ was fixed at 16 $s^{-1}$, which is the time resolution of our experiments and a lower estimate of the true value. $k^{\infty}_{undock}$ was then obtained from fitting the data with eq 2, which is not sensitive to the value of $k^{0}_{undock}$. The standard deviations reported on the Φ-values were obtained from carrying out error-propagation analysis using the uncertainties in the rate constants $k^{\infty}_{undock}$ and $k^{\infty}_{dock}$ (Tables S1 and S2) obtained from nonlinear curve fitting to eqs 1 and 2.

## ■ ASSOCIATED CONTENT

### Supporting Information

The Supporting Information is available free of charge on the ACS Publications website at DOI: 10.1021/jacs.5b09740.

Error propagation of smTSA, kinetic fit parameters, raw smFRET traces, cumulative dwell time distributions, and cross-correlation analyses (PDF)

## ■ AUTHOR INFORMATION


### Corresponding Author

*nwalter@umich.edu


### Notes

The authors declare no competing financial interest.

## ■ ACKNOWLEDGMENTS

N.G.W. thanks Prof. George Garcia for gifts of preQ$_1$ and preQ$_0$. This research was supported by the National Institutes of Health grant GM062357 and a subcontract on GM063162 to N.G.W.

## ■ REFERENCES


(1) Serganov, A.; Nudler, E. *Cell* **2013**, *152*, 17.
(2) Breaker, R. R. *Cold Spring Harbor Perspect. Biol.* **2012**, *4*, a003566.
(3) Peselis, A.; Serganov, A. *Biochim. Biophys. Acta, Gene Regul. Mech.* **2014**, *1839*, 908.
(4) Haller, A.; Souliere, M. F.; Micura, R. *Acc. Chem. Res.* **2011**, *44*, 1339.
(5) Savinov, A.; Perez, C. F.; Block, S. M. *Biochim. Biophys. Acta, Gene Regul. Mech.* **2014**, *1839*, 1030.
(6) Hammes, G. G.; Chang, Y. C.; Oas, T. G. *Proc. Natl. Acad. Sci. U. S. A.* **2009**, *106*, 13737.
(7) Hatzakis, N. S. *Biophys. Chem.* **2014**, *186*, 46.
(8) Vogt, A. D.; Di Cera, E. *Biochemistry* **2012**, *51*, 5894.
(9) Kim, E.; Lee, S.; Jeon, A.; Choi, J. M.; Lee, H. S.; Hohng, S.; Kim, H. S. *Nat. Chem. Biol.* **2013**, *9*, 313.
(10) Gouridis, G.; Schuurman-Wolters, G. K.; Ploetz, E.; Husada, F.; Vietrov, R.; de Boer, M.; Cordes, T.; Poolman, B. *Nat. Struct. Mol. Biol.* **2015**, *22*, 57.
(11) Suddala, K. C.; Walter, N. G. *Methods Enzymol.* **2014**, *549*, 343.
(12) Bae, S.; Kim, D.; Kim, K. K.; Kim, Y. G.; Hohng, S. *J. Am. Chem. Soc.* **2011**, *133*, 668.
(13) Roth, A.; Winkler, W. C.; Regulski, E. E.; Lee, B. W.; Lim, J.; Jona, I.; Barrick, J. E.; Ritwik, A.; Kim, J. N.; Welz, R.; Iwata-Reuyl, D.; Breaker, R. R. *Nat. Struct. Mol. Biol.* **2007**, *14*, 308.
(14) Roy, R.; Hohng, S.; Ha, T. *Nat. Methods* **2008**, *5*, 507.
(15) Durand, J. M.; Okada, N.; Tobe, T.; Watarai, M.; Fukuda, I.; Suzuki, T.; Nakata, N.; Komatsu, K.; Yoshikawa, M.; Sasakawa, C. *J. Bacteriol.* **1994**, *176*, 4627.
(16) Fergus, C.; Barnes, D.; Alqasem, M. A.; Kelly, V. P. *Nutrients* **2015**, *7*, 2897.
(17) Kang, M.; Peterson, R.; Feigon, J. *Mol. Cell* **2009**, *33*, 784.
(18) Klein, D. J.; Edwards, T. E.; Ferré-D'Amaré, A. R. *Nat. Struct. Mol. Biol.* **2009**, *16*, 343.
(19) Jenkins, J. L.; Krucinska, J.; McCarty, R. M.; Bandarian, V.; Wedekind, J. E. *J. Biol. Chem.* **2011**, *286*, 24626.
(20) Eichhorn, C. D.; Kang, M.; Feigon, J. *Biochim. Biophys. Acta, Gene Regul. Mech.* **2014**, *1839*, 939.
(21) Suddala, K. C.; Rinaldi, A. J.; Feng, J.; Mustoe, A. M.; Eichhorn, C. D.; Liberman, J. A.; Wedekind, J. E.; Al-Hashimi, H. M.; Brooks, C. L., 3rd; Walter, N. G. *Nucleic Acids Res.* **2013**, *41*, 10462.
(22) Misra, V. K.; Draper, D. E. *Biopolymers* **1998**, *48*, 113.
(23) Santner, T.; Rieder, U.; Kreutz, C.; Micura, R. *J. Am. Chem. Soc.* **2012**, *134*, 11928.
(24) Weikl, T. R.; Paul, F. *Protein Sci.* **2014**, *23*, 1508.




DOI: 10.1021/jacs.5b09740
J. Am. Chem. Soc. 2015, 137, 14075−14083

(25) Daniels, K. G.; Tonthat, N. K.; McClure, D. R.; Chang, Y. C.; Liu, X.; Schumacher, M. A.; Fierke, C. A.; Schmidler, S. C.; Oas, T. G. *J. Am. Chem. Soc.* **2014**, *136*, 822.
(26) Bokinsky, G.; Rueda, D.; Misra, V. K.; Rhodes, M. M.; Gordus, A.; Babcock, H. P.; Walter, N. G.; Zhuang, X. *Proc. Natl. Acad. Sci. U. S. A.* **2003**, *100*, 9302.
(27) Fersht, A. R.; Sato, S. *Proc. Natl. Acad. Sci. U. S. A.* **2004**, *101*, 7976.
(28) Dogan, J.; Mu, X.; Engstrom, A.; Jemth, P. *Sci. Rep.* **2013**, *3*, 2076.
(29) Silverman, S. K.; Cech, T. R. *RNA* **2001**, *7*, 161.
(30) Gianni, S.; Dogan, J.; Jemth, P. *Intrinsically Disordered Proteins* **2014**, *2*, 1.
(31) Fersht, A. R.; Daggett, V. *Cell* **2002**, *108*, 573.
(32) Rogers, J. M.; Oleinikovas, V.; Shammas, S. L.; Wong, C. T.; De Sancho, D.; Baker, C. M.; Clarke, J. *Proc. Natl. Acad. Sci. U. S. A.* **2014**, *111*, 15420.
(33) Giri, R.; Morrone, A.; Toto, A.; Brunori, M.; Gianni, S. *Proc. Natl. Acad. Sci. U. S. A.* **2013**, *110*, 14942.
(34) Garst, A. D.; Batey, R. T. *Biochim. Biophys. Acta, Gene Regul. Mech.* **2009**, *1789*, 584.
(35) Liberman, J. A.; Wedekind, J. E. *Wiley Interdiscip Rev. RNA* **2012**, *3*, 369.
(36) Moschen, T.; Wunderlich, C. H.; Spitzer, R.; Levic, J.; Micura, R.; Tollinger, M.; Kreutz, C. *Angew. Chem., Int. Ed.* **2015**, *54*, 560.
(37) Buck, J.; Wacker, A.; Warkentin, E.; Wohnert, J.; Wirmer-Bartoschek, J.; Schwalbe, H. *Nucleic Acids Res.* **2011**, *39*, 9768.
(38) Fiegland, L. R.; Garst, A. D.; Batey, R. T.; Nesbitt, D. J. *Biochemistry* **2012**, *51*, 9223.
(39) Zhang, Q.; Kang, M.; Peterson, R. D.; Feigon, J. *J. Am. Chem. Soc.* **2011**, *133*, 5190.
(40) Rieder, U.; Lang, K.; Kreutz, C.; Polacek, N.; Micura, R. *ChemBioChem* **2009**, *10*, 1141.
(41) Daniels, K. G.; Suo, Y.; Oas, T. G. *Proc. Natl. Acad. Sci. U. S. A.* **2015**, *112*, 9352.
(42) Hyeon, C.; Lee, J.; Yoon, J.; Hohng, S.; Thirumalai, D. *Nat. Chem.* **2012**, *4*, 907.
(43) Kowerko, D.; Konig, S. L. B.; Skilandat, M.; Kruschel, D.; Hadzic, M. C. A. S.; Cardo, L.; Sigel, R. K. O. *Proc. Natl. Acad. Sci. U. S. A.* **2015**, *112*, 3403.
(44) Zhuang, X.; Kim, H.; Pereira, M. J.; Babcock, H. P.; Walter, N. G.; Chu, S. *Science* **2002**, *296*, 1473.
(45) Vogt, A. D.; Pozzi, N.; Chen, Z.; Di Cera, E. *Biophys. Chem.* **2014**, *186*, 13.
(46) Holmstrom, E. D.; Polaski, J. T.; Batey, R. T.; Nesbitt, D. J. *J. Am. Chem. Soc.* **2014**, *136*, 16832.
(47) Aitken, C. E.; Marshall, R. A.; Puglisi, J. D. *Biophys. J.* **2008**, *94*, 1826.
(48) Qin, F.; Li, L. *Biophys. J.* **2004**, *87*, 1657.
(49) Blanco, M.; Walter, N. G. *Methods Enzymol.* **2010**, *472*, 153.
(50) Ragunathan, K.; Liu, C.; Ha, T. *eLife* **2012**, *1*, e00067.


DOI: 10.1021/jacs.5b09740
*J. Am. Chem. Soc.* 2015, 137, 14075−14083